BULLETIN OF THE POLISH ACADEMY OF SCIENCES
TECHNICAL SCIENCES, Vol. 66, No. 2, 2018
DOI: 10.24425/122104

Finger joint synovitis detection in ultrasound images

K. RADLAK, M. FRACKIEWICZ*, H. PALUS, and B. SMOLKA

Silesian University of Technology, ul. Akademicka 16, 44-100 Gliwice, Poland

Abstract. Ultrasonography has proved its usefulness in the evaluation of joint inflammations caused by rheumatoid arthritis. The illness severity is scored by human examiners based on their experience, but some discrepancies in the final diagnosis and treatment frequently occur. Therefore, the main aim of this work is the elaboration of an automatic method of the localization of finger joint inflammation level in ultrasound images. In this paper we propose a novel, fully automated framework for synovitis region segmentation. In our approach we compare several bones and joint localization methods based on the seeded region growing technique, which is combined with different speckle noise filtering algorithms. This technique extracts a region from the image using some predefined criteria of similarity between initially selected point and the pixels in its neighborhood. The seed point is localized automatically as the darkest patch within a small region between two detected finger bones close to the joint. The region affected by synovitis is found using the adopted criterion of homogeneity based on a patch to patch similarity measure. The obtained results exhibit a satisfying accuracy in comparison with the annotations prepared by an expert and the results delivered by semi-automatic methods that require manual bones delineation.

Key words: synovitis, finger joint, seeded region growing, ultrasound imaging, image segmentation.

1. Introduction

Ultrasound imaging (US) is an inexpensive and real time method used for human body structures visualisation. This technique is also a very sensitive imaging modality that facilitates an accurate diagnosis at the early stages of rheumatoid arthritis (RA) and makes it possible to monitor the responses to the applied therapies [1]. Although its initial use was limited to the inspection of larger joints, the latest improvements in image resolution and contrast have enabled the evaluation of smaller joints [2] and the detection of RA induced pathology in the early stages of the disease [1, 3].

RA is a chronic inflammatory illness, whose prevalence is estimated as being 1% of the population [4] and its early screening allows to prevent its progression. Many researchers have reported a high sensitivity of ultrasonography that is based on the detection of joint effusion, synovitis or bone erosions in joints affected by RA [1, 5, 6].

US can be used in the evaluation of synovitis, which is a sensitive marker of disease activity and severity in RA. However, there are some discrepancies in the final diagnosis and treatment regarding its validity and reproducibility, especially between different examiners. It is worth to notice that according to the research conducted by D'Agostino et al. [7] the proportions of agreement between fellow and senior radiologists in tagging images depicting synovitis or not is equal to 42% at the first evaluation, and rose progressively to 82% after 70 examinations. It shows that even the radiologists may experience problems with accurate evaluation of this type of data.

Synovitis is defined as an inflammation of the synovial membrane and is a characteristic symptom of RA [8]. Synovial changes are scored from 0 to 3 by radiologists or trained rheumatologists based on their experience or by using standardised atlases [9, 10]. According to this semiquantitative scoring system, 0 means no pathological changes and 3 denotes synovial thickening that bulges over the line that links the tops of the periarticular bones with extension to at least one of the bone diaphyses [1]. However, such an evaluation of the disease involves some degree of subjectivity and therefore an automated method for the assessment of joint inflammation level in RA using ultrasound images needs to be developed. Exemplary ultrasound images with different degrees of synovitis and manually marked ROIs (regions of interest) are presented in Fig. 1.

The degree of synovitis can be assessed by estimating the size of the dark area above the finger bones or the joint using a computer program. Consequently, the task of the automated determination of the level of synovitis can be considered as a problem of segmentation of low intensity image regions in the vicinity of the bones and the joint. In order to determine the synovitis position on the image domain, it is necessary to detect the bone, skin and joint to limit the ROI.

Among different image segmentation methods, four classes can be distinguished: pixel-based, region-based, contour-based and hybrid methods. In the category of region-based segmentation algorithms, the region growing technique plays an important role. It can be implemented in two versions: with seeds to start the segmentation and without seeds, using the pixel aggregation. In this work, we have applied seeded region growing (SRG) method introduced in [11] in order to detect the synovitis

*e-mail: mariusz.frackiewicz@polsl.pl

Manuscript submitted 2017-02-14, revised 2017-05-25, initially accepted for publication 2017-08-10, published in April 2018.

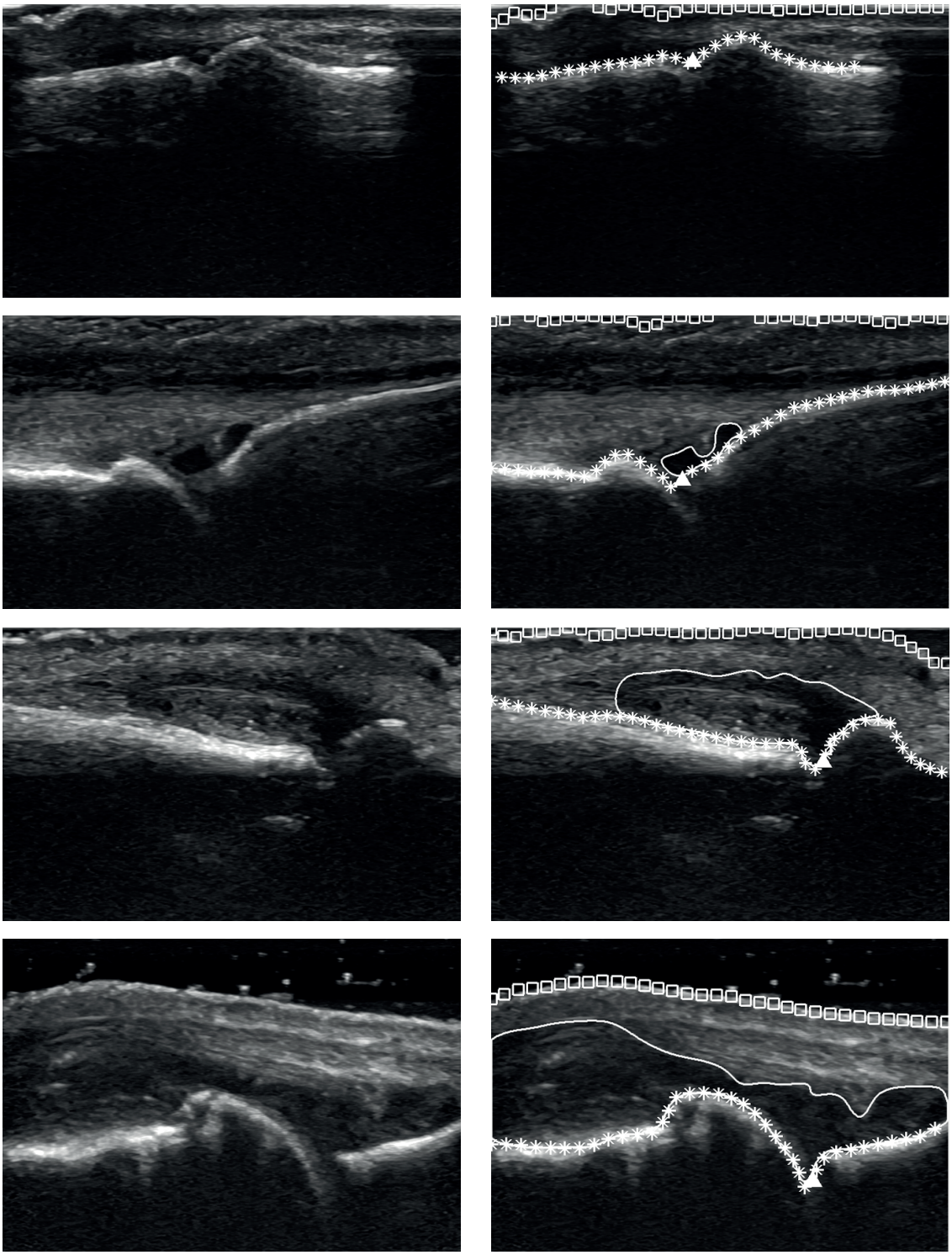

Fig. 1. Ultrasound images on the left and a manually delineated synovial region (solid line), bones (asterisks), skin (squares) and joint (triangle) on the right. The subsequent rows illustrate the level of synovitis in RA from 0 to 3

region in ultrasound images. In this technique, an initial pixel known as seed is chosen and then at each step of the algorithm a pixel in a small neighborhood, for which the difference in intensity levels to the initial pixel is smaller than a predefined threshold is attached to the expanding region. This threshold is an important parameter of this algorithm. The initial seed is typically chosen manually, but in our work it is localized automatically as the darkest patch in a small neighborhood of the joint limited by the bones edges.

In this work, we analyze the accuracy of bones and joint localization for final synovitis segmentation using two automated algorithms presented in [12, 13] and compare them with

the manually marked annotations. These algorithms can be also substituted by other currently proposed automated methods of bones, joint and skin localization [14–16].

Our main contribution is an extension of the basic SRG algorithm by applying the patch-based similarity measure instead of standard comparisons of pixel intensities. It means that a new pixel is added to the region if the patch centered at this pixel is similar to the patch centered at the initial seed. The patch-based methods are widely used in many applications such as texture synthesis [17], image denoising [18] and image segmentation [19]. We also tested the influence of several state-of-the-art speckle denosing filters on the accuracy of the synovitis segmentation.

To evaluate the novel methodology of the automated synovitis localisation, a large set of ultrasound images with manually prepared annotations was collected within the MEDUSA project[1] from patients with RA during routine visits at the Rheumatology Department of Helse Førde in Norway. The obtained results were evaluated on the MEDUSA database, which contains manually annotated markers of the bone, skin, joint and synovitis regions. This research is a preliminary step in the development of a fully automated system that will support the diagnosis of RA.

The paper is organised as follows. The next Section provides a brief description of the proposed framework for fully automated synovitis detection. Section 3 presents the numerical results of synovitis segmentation accuracy, which was evaluated on manually marked regions utilising the MEDUSA database and Section 4 concludes the paper.

2. Proposed algorithm

In this work, we propose a novel framework that allows to estimate the synovitis region in the ultrasound image. The proposed algorithm consists of several steps and the first one is the bone and joint localization. Then segmentation of the synovitis region using SRG algorithm and its modification is performed on the raw and denoised ultrasound images. Finally, the correction of the detected blobs is conducted by cutting the estimated blobs if they become very narrow, what may be interpreted as the tendon detection.

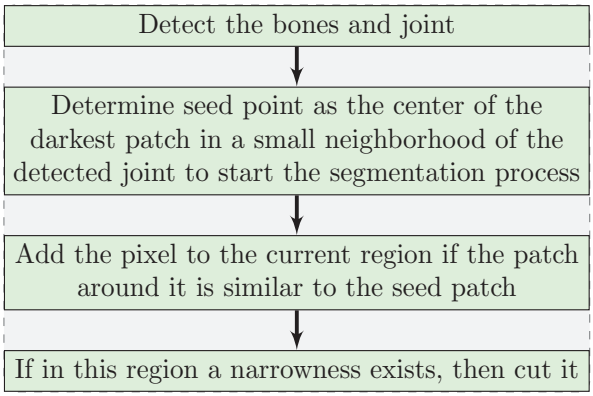

Fig. 2. The flowchart of the proposed algorithm for synovitis region extraction

The flowchart of the proposed algorithm of synovitis region detection is presented in Fig. 2.

2.1. Bones and joint localization. The first step in the proposed pipeline is the localization of 2 finger bones and the joint. Due to the fact that the physicians indicated that the inflammation of the synovial membrane develops along the bone and it starts to grow in the joint capsule causing the tissue to become swollen and painful, the precise localization of these two characteristic regions is of highest importance. Therefore, in this work, we are comparing two recently proposed automated methods of bones localization. Both algorithms are related with the observed properties of the acoustic wave. The strength of the signal transmitted from the transducer into the tissue is decreasing exponentially according to the Lambert's law and the strongest decrease is observed when the wave meets the obstacles, e.g. in form of a bone. The intensity of the signal reflected from the bones is represented by the brightest pixels, while the pixels below the bones region are darker. These properties are considered in two algorithms for automated bone localization presented in [12, 13], which are analyzed in this paper. The exemplary results of bones and joints localization that were obtained using the analyzed methods are presented in Fig. 3.

[1]MEDUSA project, http://medusa.aei.polsl.pl, Accessed: 2017–02–01

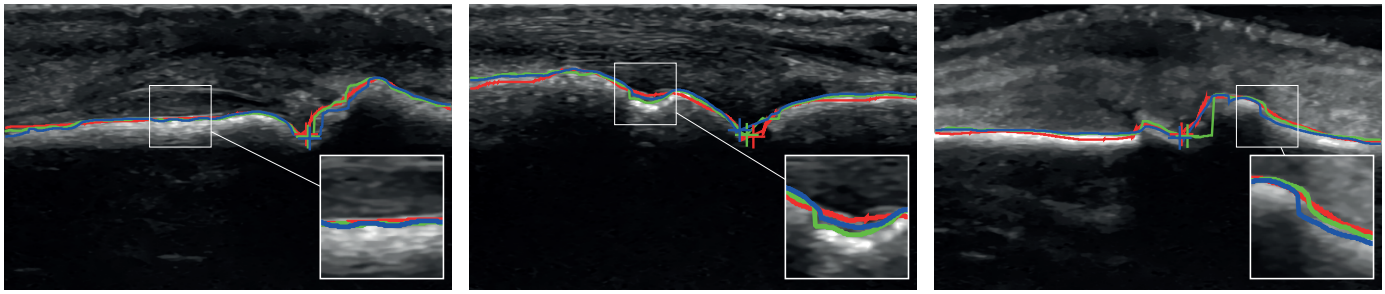

Fig. 3. Exemplary bones and joint detection – comparison of manual annotations performed by an expert (red line) with automated methods: Radlak et al. [13] (green line), Popowicz and Kurek [12] (blue line)

In the first method, the bones were localized utilizing algorithm proposed by Radlak et al. in [13]. In this approach, a modification of the concept of bone confidence localizer proposed in [20] is applied, in which from the original ultrasound image filtered using trimmed non-local means (TNLM) algorithm, the normalized values of confidence map [21] are subtracted. As a result, we obtain a map with the high response at the bone surface, because the high values in ultrasound image followed by a low confidence map intensities are a good indicator for a possible bone surface. Then, the obtained bone localization map is thresholded and two biggest blobs are detected as finger bones.

In the method proposed by Popowicz and Kurek [12], the intenisties of the original image pixels is decreased by the maximum gray level of samples located in a rectangular region below the analyzed image point. In order to diminish the artifacts in original image, the median filtering is applied. Next, the obtained image is thresholded and the largest blobs are selected as final bones region and all pixels below and above these regions are removed from further analysis.

In our pipeline, the joint is localized utilizing the concept presented in [12], so that the joint position is estimated as the maximum in the signal obtained by calculating the difference between the y-coordinates of currently processed pixel of bone surface and the sum of the maximum values of the pixels on the left and right sides.

2.2. Speckle noise reduction. In computer vision systems we usually are dealing with images distorted by noise. In digital images, there are many types of noise e.g Gaussian noise, salt and pepper noise, shot noise, film grain, anisotropic noise, etc. The noise also relates to a device for image acquisition e.g. effects of sensor size, fill factor, temperature, etc. The occurrence of noise in images makes their analysis difficult and may lead to incorrect medical imaging diagnosis. In the USG we have to deal with the speckle noise which is a granular disturbance and severely degrades the quality of USG images. To minimize the effect of noise, edge preserving smoothing is performed with the previously selected filter corresponding to the type of distortion.

In this article the following filters were used for evaluation purposes: Wiener Filter [22], speckle reducing anisotropic diffusion (SRAD) [23], non-local means (NLM) [24], optimized Bayesian non-local means (OBNLM) [25], probabilistic patch-based weights (PPBW) [26] and trimmed nonlocal means (TNLM) [27]. The application of these methods requires a proper setting of the parameters according to the suggestions of their authors. Examples of some filtering results are shown in Fig. 4, in which a part of the test images was cropped and zoomed. As can be observed, using the TNLM filter the bone boundary becomes sharper sharper and synovial region is quite homogeneous. Filtering quality was evaluated in Section 3 in terms of the final results of segmentation utilizing quality indices.

2.3. Seeded region growing segmentation. Segmentation is the process of image division into regions with similar properties such as gray level, color, texture, brightness or contrast [28]. The basic segmentation techniques can be divided into several groups: thresholding, clustering, region growing, edge detection, active contour, etc. [29, 30]. The role of segmentation is to identify homogeneous regions in an image that represent objects or their meaningful parts. Automatic segmentation of ultrasound images is a difficult task due to the complex nature of this kind of data and the influence of speckle noise. Further, the output of any segmentation algorithm is affected by: (i) partial volume effect, (ii) intensity inhomogeneity, (iii) presence of similar gray levels of different soft tissues [28]. In the rich literature hundreds of methods have been proposed, but none of these techniques can be considered as universal for different type of images and very often a single algorithm does not work well for an image class for which it was developed.

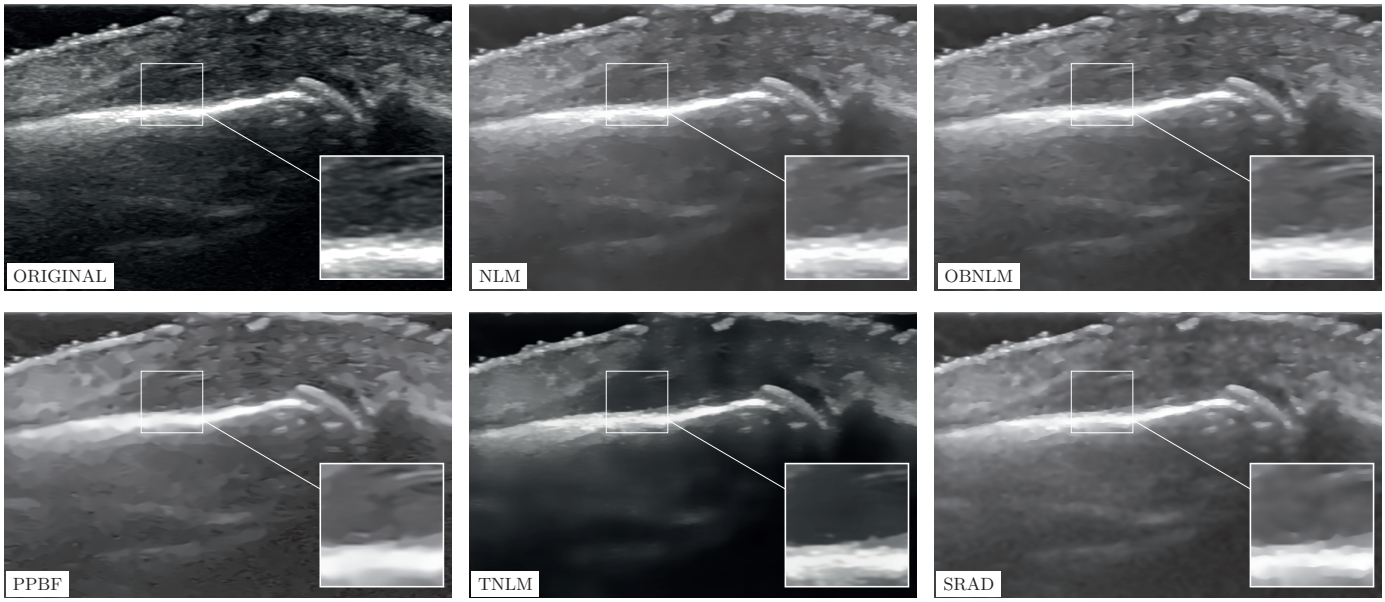

Fig. 4. Comparison of the noise filtering results

Fig. 5. Example of the division of the segmented region. The red color depicts the left profile of the blob (blue is used for the right one) and the plus sign denotes the detected local extremum in the left and right boundary of the blob transformed to 1 D. The cyan represents the line, where the blob is cut off

Region growing method is a technique that extracts a region from the image using some predefined homogeneity criteria. It is a typical bottom-up technique. The easiest way is to select the seed point manually, attaching to it the next pixel on the basis of the adopted criterion of homogeneity and updating the obtained region attributes (e.g. average intensity, area etc.). The choice of homogeneity criterion is therefore crucial for the success of segmentation. The seed can be selected manually or semi-manually (seeded region growing method, eg. [11]) or in an automatic way (unseeded region growing method, e.g. [31]).

Seeded region growing method was initially proposed in [11] and its features such as robustness, low computational complexity, lack of tuning parameters makes it suitable for large range of images. In this approach, initially the seeds or regions are to be specified by the user. The choice of the seed is very crucial, since the overall success of the segmentation is dependent on the seed input. For the given set of seeds, the algorithm adds pixels to one of them. The input seed points can be determined automatically for example as the centroids of the segmented regions obtained using other type of segmentation algorithm. Next, the pixels are connected to the seeds using some predefined criteria. The simplest criterion might be to grow the region until the difference in intensity level between the new pixel and the seed is below an assumed threshold. During the growing process the concept of 4-connectivity or 8-connectivity can be used.

In this work we tested the basic seeded region growing algorithm adjusted for the finger ultrasound images and we chose only the single seed point within the inflammation area as the pixel for which the patch centered at this pixel has the lowest sum of the intensity levels. This algorithm is defined as follows:

1. Determine seed points to start the segmentation process.
2. Add the pixel in the neighborhood to the current region if all conditions are fulfilled:
   a) the pixel intensity is within the range of the assumed threshold,
   b) the spatial distance between the analyzed pixel and the seed does not exceed a predefined maximum value,
   c) the region can grow up only in limited range, this assumption is based on the physical properties of this kind of ultrasound images, because the texture below the bones should be treated as noise.
4. Finally fill the holes in the generated region.

This algorithm can be extended introducing a patch comparison instead of simple pixel intensities analysis. In this approach local intensity context around the pixel can be used to perform a robust comparison of samples.

Let us consider an ultrasound image I as a set of pixels x_i, where i determines the position of the pixel on the image domain, $i = 1, 2, \ldots, N$, and N denotes the number of image pixels. Let x_s represent the pixel chosen as the seed and R denotes the segmented synovitis region. Let $W_i = (x_{i,1}, x_{i,2}, \ldots, x_{i,n})$ stands for the set of pixels from a small square window centered at pixel x_i, with n denoting the number of pixels and p denoting the size of the patch W_i so that $n = p \times p$. We tested three patch sizes: $n = 1 \times 1$ for SRG method, $n = 3 \times 3$ for $\mathrm{SRG}_{3\times3}$ and $n = 5 \times 5$ for $\mathrm{SRG}_{5\times5}$ method. The distance $d(W_i, W_s)$ between patches W_i and W_s is defined as

$$d(W_i, W_s) = \frac{1}{n}\sum_{j}^{n} |x_{i,j} - x_{s,j}|. \tag{1}$$

In the proposed modification, a new pixel x_i is attached to the region R if $d(W_i, W_s) < t$, where t is some predefined threshold. In this way, we consider not only the pixel intensity, but we also take into account the texture properties in the vicinity of the seed and the currently processed pixel.

2.4. Tendon line estimation. In our work, we also noticed that sometimes the segmentation of finger joints depicted in ultrasound images is very hard, because the textural properties of the synovitis and the region near the skin are almost the same and they are merged by the algorithm. To cope with this artifact, we found that we are able to cut the obtained blob based on its contour profile. As has been presented in Fig. 5, the detected region

can be cut at points, in which the strongest narrowness between the left and right blob edges is observed. The transformation of the boundary to the 1D function is defined as the maximal column index for left profile and minimum column index for the right profile in each row. Therefore, the search for the points, in which the blob will be cut was reduced to the problem of searching for the local minima and maxima of 1D function. To recognize if the division is necessary, we also assume that the difference between the lowest extremum (depends on which side of contour is analyzed) and the extrema in their neighborhood have to be bigger than a predefined threshold. In this work we use a fixed value of threshold, which is equal to 20, assuming 8-bit image. This post-processing step significantly improves the localization of the synovitis region by removing the incorrect part of the detected blob.

The border of the synovitis region is also limited along the tendon line by physicians in their analysis, however this structure was not annotated in the MEDUSA database. Thus, this post-processing procedure can be used for the tendon localization.

2.5. Segmentation evaluation. The evaluation of segmentation methods typically involves comparing the results obtained with the manual segmentation carried out by an expert [32, 33]. To evaluate the obtained segmentation results we used two similarity coefficient indices: Jaccard's similarity coefficient [34]:

$$J(I_{seg}, I_{ref}) = \frac{|I_{seg} \cap I_{ref}|}{|I_{seg} \cup I_{ref}|}, \tag{2}$$

and Dice's similarity coefficient (Sørensen index) [35, 36]:

$$D(I_{seg}, I_{ref}) = \frac{2|I_{seg} \cap I_{ref}|}{|I_{seg}| + |I_{ref}|}, \tag{3}$$

where: $|I_{seg} \cap I_{ref}|$ denotes the area of the intersection between automatically and manually delineated synovial region, $|I_{seg} \cup I_{ref}|$ is the size of their union. $|I_{seg}|$ and $|I_{ref}|$ are the number of pixels in these two regions. Both similarity coefficients have a range of 0 to 1 with higher scores indicating better segmentation result.

3. Results

In this paper, we tested our automated segmentation methods on images from the MEDUSA project. The database contains 267 images with manually annotated bones, joint, skin and synovitis region. The proposed segmentation methods was compared with manually delineated synovial regions. The images were acquired using the LOGIQ S8 by GE Healthcare (USA) with 8 bit depth.

We examined the influence of several parameters on segmentation accuracy: the choice of the denoising algorithm, bone and joint detection methods and parameters connected with SRG algorithm (threshold t and size of the of the processing window p). The results of these tests were evaluated using the Dice and Jaccard indices. The influence of these factors on Dice index for different filtering algorithms is shown in Fig. 6.

Some results with the highest Jaccard and Dice indices are presented in Fig. 7, where the obtained regions of RA are very close to manually delineated areas. Three segmentation results of RA are presented: manually delineated regions, semi-automated segmentation and automated segmentation. For semi-automated segmentation we used bones and joint localization performed by an expert. In automated segmentation method, localization of bones and joint are found automatically based on the method proposed by Radlak et al. [13]. The results of both automatic detection methods of the joint and the bones are very close to the manual annotations and allow to obtain satisfying results. However, the application of confidence map slightly increases the segmentation quality indices.

The results obtained with semi-automated segmentation method based on manually annotated bones and joint are slightly better than the fully automated methods based on automatically localized bones and joint. The t parameter providing the highest Dice index is dependent on the applied filtering algorithms and size of patch p. We tested the t parameter values from 25 to 65. Detailed Dice and Jaccard indices for the range of t parameter from 35 to 45 are shown in Tabs 1, 2. Outside this range both index values were smaller. For the six tested filters, the TNLM filter most improves the segmentation result for the SRG and the t parameter equal 35. With the increase of the t parameter, the TNLM filtering stops correcting the index values. In the absence of filtering, the increase of the t parameter results in an improvement of index values for all cases. Tables 1, 2 contain the average values and 95% confidence intervals for Dice and Jaccard indices for all tested filtering algorithms and segmentation methods.

For the basic SRG method with manually annotated bones we obtained the best mean Dice index equal to 0.684 and Jaccard index equal to 0.552 using TNLM filter. The application of the automated bones and joint detection methods causes that the best mean Dice index decreased to 0.617 and Jaccard index to 0.486. The proposed patch-based modification of SRG algorithm improves the segmentation results mainly for unfiltered images. The use of image filtering removes speckle noise, smoothes texture and enhances boundaries of the synovial region. Therefore the proposed modification of the SRG algorithm improves the results only for the raw, unfiltered images.

Figure 8 presents difficult cases for segmentation where we obtained lowest similarity coefficients. This situation occurs for both the original and filtered images.

4. Conclusions

This work presents a novel fully automated approach to the synovitis segmentation, which is based on the basic seeded

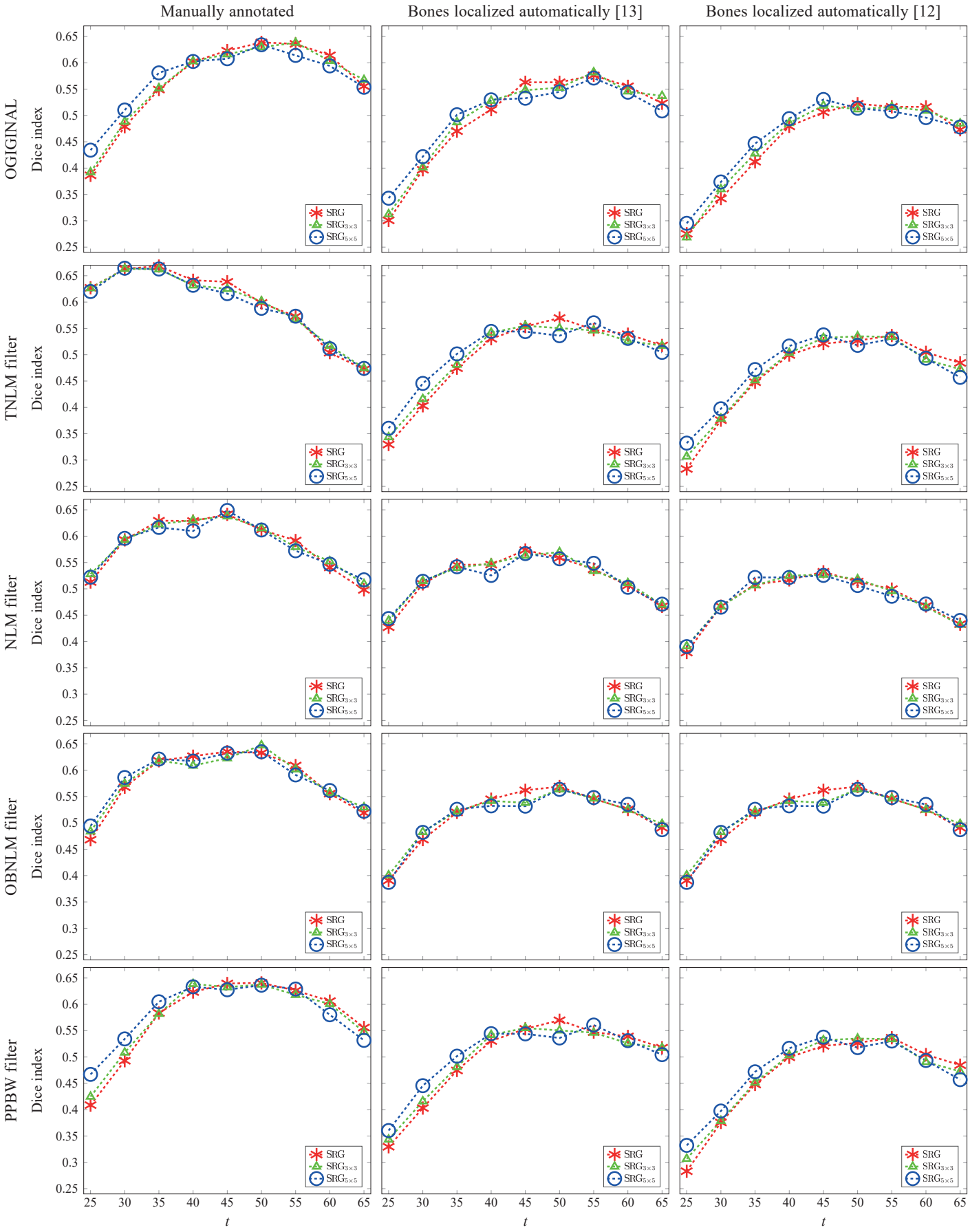

Fig. 6. Influence of the threshold t on mean values of Dice index

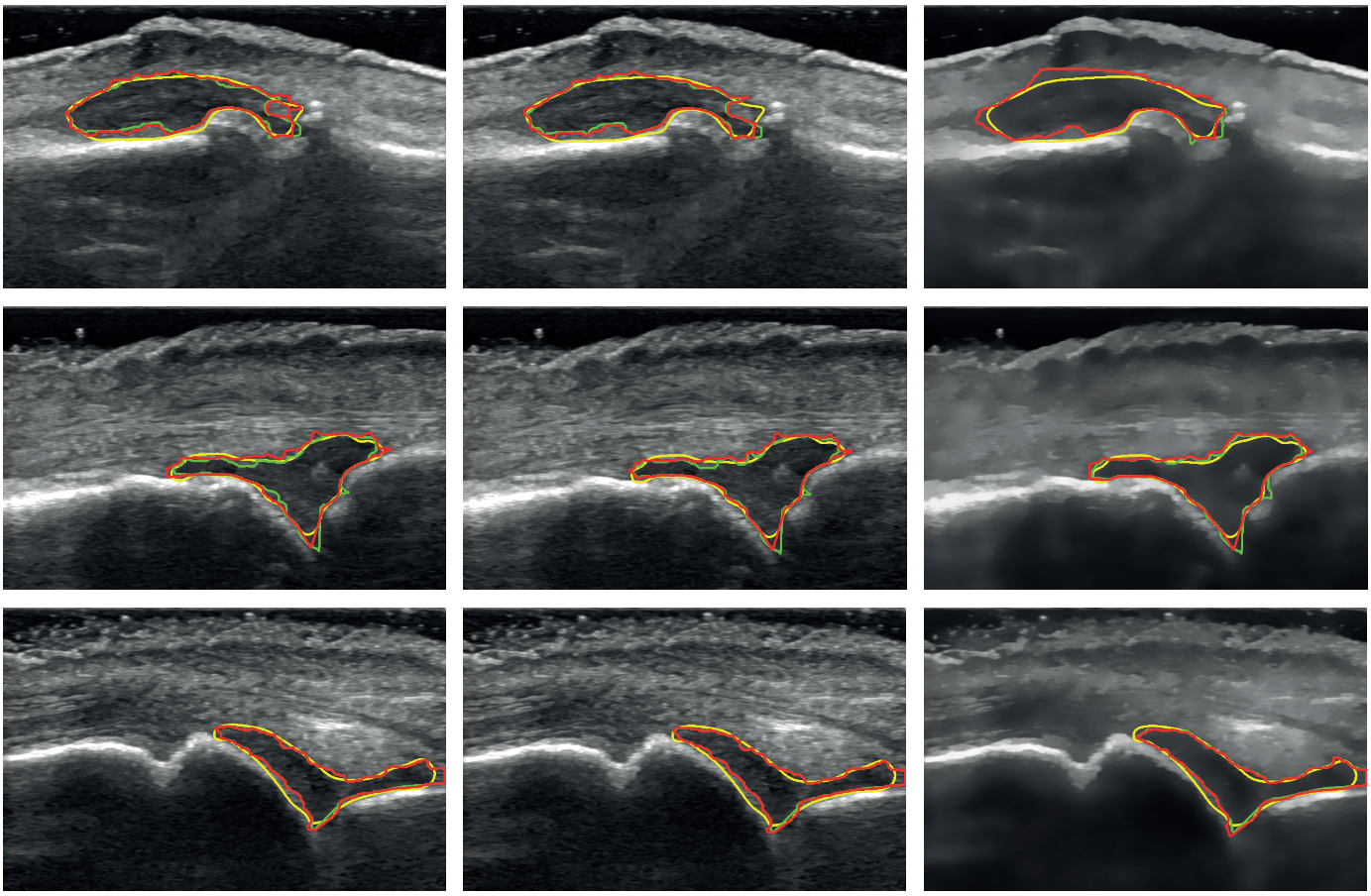

Fig. 7. Comparison of manually delineated regions (yellow lines) with semi-automated segmentation (red line) and with automated segmentation results of RA (green line). The subsequent rows illustrate different US images and subsequent columns illustrate methods: ORIGINAL & $SRG_{1\times1}$, ORIGINAL & $SRG_{5\times5}$, TNLM & $SRG_{1\times1}$

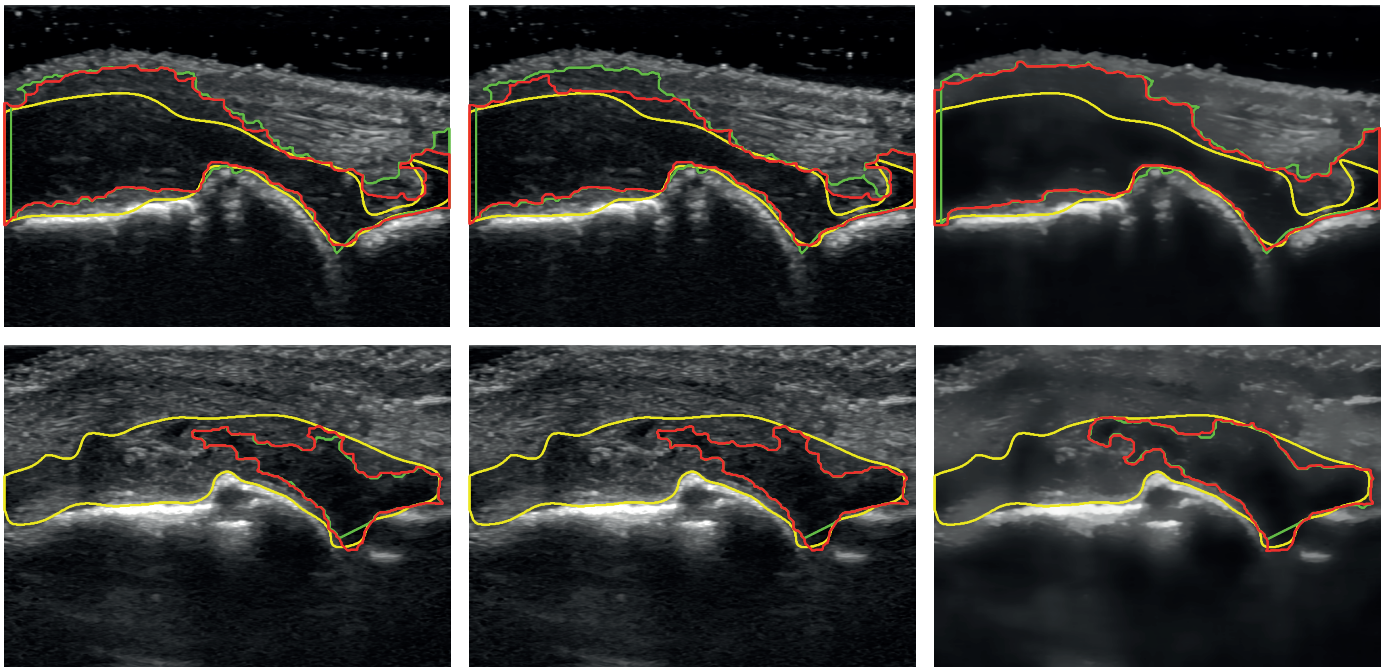

Fig. 8. Examples of manually delineated regions of RA (yellow lines) with semi-automated segmentation (red line) and with automated segmentation results of RA (green line). The subsequent rows illustrate different US images and subsequent columns illustrate methods: ORIGINAL &, ORIGINAL & $SRG_{5\times5}$, TNLM & $SRG_{1\times1}$

Table 1
Mean value of Dice index and confidence intervals for segmentation of original and filtered images from the MEDUSA database using manual and automated bones and joint localization for different values of threshold t

	Manual			Radlak et al. [13]			Popowicz and Kurek [12]		
	SRG	$SRG_{3\times3}$	$SRG_{5\times5}$	SRG	$SRG_{3\times3}$	$SRG_{5\times5}$	SRG	$SRG_{3\times3}$	$SRG_{5\times5}$
					$t = 35$				
ORIGINAL	0.590 ± 0.025	0.600 ± 0.024	0.615 ± 0.023	0.514 ± 0.027	0.530 ± 0.025	0.544 ± 0.025	0.472 ± 0.029	0.475 ± 0.029	0.506 ± 0.028
TNLM	0.684 ± 0.020	0.680 ± 0.020	0.677 ± 0.020	0.617 ± 0.025	0.602 ± 0.025	0.598 ± 0.025	0.570 ± 0.028	0.557 ± 0.028	0.558 ± 0.028
NLM	0.656 ± 0.021	0.654 ± 0.021	0.646 ± 0.023	0.589 ± 0.025	0.587 ± 0.025	0.586 ± 0.026	0.547 ± 0.028	0.546 ± 0.028	0.548 ± 0.028
OBNLM	0.649 ± 0.021	0.643 ± 0.022	0.650 ± 0.021	0.570 ± 0.026	0.558 ± 0.027	0.569 ± 0.026	0.533 ± 0.028	0.525 ± 0.029	0.533 ± 0.029
PPBW	0.614 ± 0.025	0.617 ± 0.025	0.642 ± 0.021	0.532 ± 0.027	0.547 ± 0.027	0.565 ± 0.025	0.499 ± 0.029	0.499 ± 0.029	0.518 ± 0.029
SRAD	0.664 ± 0.019	0.658 ± 0.020	0.659 ± 0.020	0.580 ± 0.025	0.575 ± 0.026	0.574 ± 0.026	0.550 ± 0.028	0.546 ± 0.028	0.541 ± 0.028
WIENER	0.624 ± 0.022	0.629 ± 0.022	0.630 ± 0.022	0.552 ± 0.025	0.561 ± 0.025	0.562 ± 0.026	0.504 ± 0.029	0.512 ± 0.028	0.519 ± 0.028
					$t = 40$				
ORIGINAL	0.626 ± 0.022	0.634 ± 0.022	0.643 ± 0.022	0.552 ± 0.026	0.566 ± 0.026	0.578 ± 0.025	0.528 ± 0.028	0.530 ± 0.028	0.535 ± 0.028
TNLM	0.649 ± 0.024	0.645 ± 0.025	0.647 ± 0.024	0.585 ± 0.027	0.584 ± 0.027	0.581 ± 0.026	0.552 ± 0.028	0.545 ± 0.028	0.537 ± 0.028
NLM	0.651 ± 0.023	0.648 ± 0.024	0.635 ± 0.025	0.584 ± 0.026	0.583 ± 0.026	0.582 ± 0.026	0.545 ± 0.028	0.542 ± 0.028	0.542 ± 0.028
OBNLM	0.655 ± 0.022	0.647 ± 0.023	0.643 ± 0.024	0.591 ± 0.025	0.582 ± 0.026	0.585 ± 0.026	0.535 ± 0.029	0.542 ± 0.028	0.549 ± 0.028
PPBW	0.653 ± 0.022	0.664 ± 0.020	0.661 ± 0.020	0.581 ± 0.024	0.587 ± 0.024	0.592 ± 0.025	0.543 ± 0.028	0.548 ± 0.028	0.553 ± 0.028
SRAD	0.657 ± 0.022	0.660 ± 0.022	0.643 ± 0.025	0.585 ± 0.026	0.591 ± 0.026	0.579 ± 0.026	0.545 ± 0.028	0.543 ± 0.029	0.542 ± 0.028
WIENER	0.651 ± 0.020	0.651 ± 0.021	0.652 ± 0.021	0.580 ± 0.025	0.586 ± 0.025	0.582 ± 0.026	0.541 ± 0.027	0.541 ± 0.028	0.548 ± 0.028
					$t = 45$				
ORIGINAL	0.641 ± 0.023	0.642 ± 0.023	0.633 ± 0.025	0.582 ± 0.026	0.583 ± 0.026	0.573 ± 0.027	0.529 ± 0.029	0.539 ± 0.029	0.550 ± 0.028
TNLM	0.619 ± 0.026	0.604 ± 0.027	0.601 ± 0.027	0.567 ± 0.028	0.565 ± 0.028	0.557 ± 0.028	0.524 ± 0.028	0.510 ± 0.028	0.514 ± 0.028
NLM	0.631 ± 0.025	0.631 ± 0.025	0.635 ± 0.024	0.574 ± 0.027	0.568 ± 0.027	0.579 ± 0.026	0.526 ± 0.029	0.522 ± 0.028	0.533 ± 0.028
OBNLM	0.650 ± 0.024	0.639 ± 0.024	0.643 ± 0.024	0.595 ± 0.025	0.578 ± 0.026	0.565 ± 0.027	0.541 ± 0.028	0.537 ± 0.028	0.544 ± 0.028
PPBW	0.659 ± 0.021	0.653 ± 0.022	0.641 ± 0.025	0.589 ± 0.025	0.595 ± 0.025	0.593 ± 0.026	0.561 ± 0.027	0.561 ± 0.027	0.553 ± 0.028
SRAD	0.644 ± 0.024	0.645 ± 0.024	0.634 ± 0.025	0.581 ± 0.026	0.582 ± 0.026	0.570 ± 0.027	0.538 ± 0.028	0.546 ± 0.027	0.546 ± 0.027
WIENER	0.641 ± 0.024	0.638 ± 0.025	0.638 ± 0.025	0.591 ± 0.025	0.590 ± 0.025	0.583 ± 0.026	0.553 ± 0.028	0.548 ± 0.028	0.548 ± 0.028

Table 2
Mean value of Jaccard index and confidence intervals for segmentation of original and filtered images from the MEDUSA database using manual and automated bones and joint localization for different values of threshold t

	Manual			Radlak et al. [13]			Popowicz and Kurek [12]		
	SRG	$SRG_{3\times3}$	$SRG_{5\times5}$	SRG	$SRG_{3\times3}$	$SRG_{5\times5}$	SRG	$SRG_{3\times3}$	$SRG_{5\times5}$
					$t = 35$				
ORIGINAL	0.590 ± 0.025	0.600 ± 0.024	0.615 ± 0.023	0.514 ± 0.027	0.530 ± 0.025	0.544 ± 0.025	0.472 ± 0.029	0.475 ± 0.029	0.506 ± 0.028
TNLM	0.684 ± 0.020	0.680 ± 0.020	0.677 ± 0.020	0.617 ± 0.025	0.602 ± 0.025	0.598 ± 0.025	0.570 ± 0.028	0.557 ± 0.028	0.558 ± 0.028
NLM	0.656 ± 0.021	0.654 ± 0.021	0.646 ± 0.023	0.589 ± 0.025	0.587 ± 0.025	0.586 ± 0.026	0.547 ± 0.028	0.546 ± 0.028	0.548 ± 0.028
OBNLM	0.649 ± 0.021	0.643 ± 0.022	0.650 ± 0.021	0.570 ± 0.026	0.558 ± 0.027	0.569 ± 0.026	0.533 ± 0.028	0.525 ± 0.029	0.533 ± 0.029
PPBW	0.614 ± 0.025	0.617 ± 0.025	0.642 ± 0.021	0.532 ± 0.027	0.547 ± 0.027	0.565 ± 0.025	0.499 ± 0.029	0.499 ± 0.029	0.518 ± 0.029
SRAD	0.664 ± 0.019	0.658 ± 0.020	0.659 ± 0.020	0.580 ± 0.025	0.575 ± 0.026	0.574 ± 0.026	0.550 ± 0.028	0.546 ± 0.028	0.541 ± 0.028
WIENER	0.624 ± 0.022	0.629 ± 0.022	0.630 ± 0.022	0.552 ± 0.025	0.561 ± 0.025	0.562 ± 0.026	0.504 ± 0.029	0.512 ± 0.028	0.519 ± 0.028
					$t = 40$				
ORIGINAL	0.626 ± 0.022	0.634 ± 0.022	0.643 ± 0.022	0.552 ± 0.026	0.566 ± 0.026	0.578 ± 0.025	0.528 ± 0.028	0.530 ± 0.028	0.535 ± 0.028
TNLM	0.649 ± 0.024	0.645 ± 0.025	0.647 ± 0.024	0.585 ± 0.027	0.584 ± 0.027	0.581 ± 0.026	0.552 ± 0.028	0.545 ± 0.028	0.537 ± 0.028
NLM	0.651 ± 0.023	0.648 ± 0.024	0.635 ± 0.025	0.584 ± 0.026	0.583 ± 0.026	0.582 ± 0.026	0.545 ± 0.028	0.542 ± 0.028	0.542 ± 0.028
OBNLM	0.655 ± 0.022	0.647 ± 0.023	0.643 ± 0.024	0.591 ± 0.025	0.582 ± 0.026	0.585 ± 0.026	0.535 ± 0.029	0.542 ± 0.028	0.549 ± 0.028
PPBW	0.653 ± 0.022	0.664 ± 0.020	0.661 ± 0.020	0.581 ± 0.024	0.587 ± 0.024	0.592 ± 0.025	0.543 ± 0.028	0.548 ± 0.028	0.553 ± 0.028
SRAD	0.657 ± 0.022	0.660 ± 0.022	0.643 ± 0.025	0.585 ± 0.026	0.591 ± 0.026	0.579 ± 0.026	0.545 ± 0.028	0.543 ± 0.029	0.542 ± 0.028
WIENER	0.651 ± 0.020	0.651 ± 0.021	0.652 ± 0.021	0.580 ± 0.025	0.586 ± 0.025	0.582 ± 0.026	0.541 ± 0.027	0.541 ± 0.028	0.548 ± 0.028
					$t = 45$				
ORIGINAL	0.641 ± 0.023	0.642 ± 0.023	0.633 ± 0.025	0.582 ± 0.026	0.583 ± 0.026	0.573 ± 0.027	0.529 ± 0.029	0.539 ± 0.029	0.550 ± 0.028
TNLM	0.619 ± 0.026	0.604 ± 0.027	0.601 ± 0.027	0.567 ± 0.028	0.565 ± 0.028	0.557 ± 0.028	0.524 ± 0.028	0.510 ± 0.028	0.514 ± 0.028
NLM	0.631 ± 0.025	0.631 ± 0.025	0.635 ± 0.024	0.574 ± 0.027	0.568 ± 0.027	0.579 ± 0.026	0.526 ± 0.029	0.522 ± 0.028	0.533 ± 0.028
OBNLM	0.650 ± 0.024	0.639 ± 0.024	0.643 ± 0.024	0.595 ± 0.025	0.578 ± 0.026	0.565 ± 0.027	0.541 ± 0.028	0.537 ± 0.028	0.544 ± 0.028
PPBW	0.659 ± 0.021	0.653 ± 0.022	0.641 ± 0.025	0.589 ± 0.025	0.595 ± 0.025	0.593 ± 0.026	0.561 ± 0.027	0.561 ± 0.027	0.553 ± 0.028
SRAD	0.644 ± 0.024	0.645 ± 0.024	0.634 ± 0.025	0.581 ± 0.026	0.582 ± 0.026	0.570 ± 0.027	0.538 ± 0.028	0.546 ± 0.027	0.546 ± 0.027
WIENER	0.641 ± 0.024	0.638 ± 0.025	0.638 ± 0.025	0.591 ± 0.025	0.590 ± 0.025	0.583 ± 0.026	0.553 ± 0.028	0.548 ± 0.028	0.548 ± 0.028

region growing algorithm and bones and joint localization technique. The proposed framework allows to obtain high-quality segmentation results. For many images, the detected synovitis area coincides very well with manually delineated regions, which confirms the ability of the presented system to support the diagnosis of rheumatoid arthritis.

Acknowledgements. The research leading to these results has received funding from the Norwegian Financial Mechanism 2009–2014 under Project Contract No. Pol-Nor/204256/16/2013. Ultrasound images created for MEDUSA project at Section for Rheumatology; Department for Neurology, Rheumatology and Physical Medicine, Central Hospital, Førde, Norway. This work was also supported from statutory funds (BK/213/RAU1/2016) of the Institute of Automatic Control, Silesian University of Technology, Poland.

References

[1] M. Szkudlarek, M. Court-Payen, S. Jacobsen, M. Klarlund, H.S. Thomsen, and M. Østergaard, "Interobserver agreement in ultrasonography of the finger and toe joints in rheumatoid arthritis," *Arthritis & Rheumatism* 48 (4), 955–962, 2003.

[2] R.J. Wakefield, P.V. Balint, M. Szkudlarek, E. Filippucci, M. Backhaus, M.-A. D'Agostino, E.N. Sanchez, A. Iagnocco, W.A. Schmidt, G.A. W. Bruyn, G. Bruyn, D. Kane, P.J. O'Connor, B. Manger, F. Joshua, J. Koski, W. Grassi, M.N.D. Lassere, N. Swen, F. Kainberger, A. Klauser, M. Ostergaard, A.K. Brown, K.P. Machold, P.G. Conaghan, and O.S.I. Group, "Musculoskeletal ultrasound including definitions for ultrasonographic pathology.," *The Journal of Rheumatology* 32 (12), 2485–2487, 2005.

[3] Y.K. Tan, M. Østergaard, and P.G. Conaghan, "Imaging tools in rheumatoid arthritis: ultrasound vs magnetic resonance imaging," *Rheumatology* 51 (7), vii36–vii42, 2012.

[4] A. Gibofsky, "Overview of epidemiology, pathophysiology, and diagnosis of rheumatoid arthritis," *American Journal of Managed Care* 18 (13), S295–S302, 2012.

[5] C.F. Arend, "Ultrasonography in rheumatoid arthritis: What rheumatologists should know," *Revista Brasileira de Reumatologia* (*English Edition*) 53 (1), 88–100, 2013.

[6] D. Ten Cate, J. Luime, N. Swen, A. Gerards, M.De Jager, N. Basoski, J. Hazes, C. Haagsma, and J. Jacobs, "Role of ultrasonography in diagnosing early rheumatoid arthritis and remission of rheumatoid arthritis – a systematic review of the literature," *Arthritis Research & Therapy* 15 (1), R4, 2013.

[7] M.-A. D'Agostino, J.-F. Maillefert, R. Said-Nahal, M. Breban, P. Ravaud, and M. Dougados, "Detection of small joint synovitis by ultrasonography: the learning curve of rheumatologists," *Annals of the Rheumatic Diseases* 63 (10), 1284–1287, 2004.

[8] J. Sokolove and C.M. Lepus, "Role of inflammation in the pathogenesis of osteoarthritis: latest findings and interpretations," *Therapeutic Advances in Musculoskeletal Disease*, 2013.

[9] M. Kulbacki, J. Segen, P. Habela, M. Janiak, W. Knieć, M. Fojcik, P. Mielnik, and K. Wojciechowski, "Collaborative tool for annotation of synovitis and assessment in ultrasound images," in *Computer Vision and Graphics* 8671 of *LNCS*, 364–373, 2014.

[10] L. Terslev, S. Torp-Pedersen, A. Savnik, P. von der Recke, E. Qvistgaard, B. Danneskiold-Samsøe, and H. Bliddal, "Doppler ultrasound and magnetic resonance imaging of synovial inflammation of the hand in rheumatoid arthritis: A comparative study," *Arthritis & Rheumatism* 48 (9), 2434–2441, 2003.

[11] R. Adams and L. Bischof, "Seeded region growing," *IEEE Transactions on Pattern Analysis and Machine Intelligence* 16 (6), 641–647, 1994.

[12] A. Popowicz and A. Kurek, "An algorithm for joint and bone localization in usg images of rheumatoid arthritis," *Studia Informatica* 37 (3B), 2016.

[13] K. Radlak, N. Radlak, and B. Smolka, "Automatic detection of bones based on the confidence map for rheumatoid arthritis analysis," in *Computational Vision and Medical Image Processing*, 215–220, Taylor & Francis Group, 2015.

[14] K. Nurzynska and B. Smolka, "Automatic finger joint synovitis localization in ultrasound images," in *Proc. SPIE 9897, Real-Time Image and Video Processing*, 98970N, 2016.

[15] M.S. Sultan, N. Martins, M.J. Ferreira, and M.T. Coimbra, "Metacarpal & phalange bones segmentation from ultrasound images," in *21st Edition of the Portuguese Conference on Pattern Recognition*, 116–17, 2015.

[16] K. Wereszczyński, J. Segen, M. Kulbacki, P. Mielnik, M. Fojcik, and K. Wojciechowski, "Identifying a joint in medical ultrasound images using trained classifiers," in *Computer Vision and Graphics* 8671 of LNCS, 626–635, Springer International Publishing, 2014.

[17] A.A. Efros and W.T. Freeman, "Image quilting for texture synthesis and transfer," in *Proceedings of the 28th Annual Conference on Computer Graphics and Interactive Techniques*, SIGGRAPH' 01, 341–346, ACM, 2001.

[18] A. Buades, B. Coll, and J.-M. Morel, "A non-local algorithm for image denoising," in *IEEE Computer Society Conference on Computer Vision and Pattern Recognition* 2, 60–65, 2005.

[19] L. Wolf, X. Huang, I. Martin, and D. Metaxas, *Patch-Based Texture Edges and Segmentation*, 481–493. Springer Berlin Heidelberg, 2006.

[20] W. Wein, A. Karamalis, A. Baumgartner, and N. Navab, "Automatic bone detection and soft tissue aware ultrasound–ct registration for computer-aided orthopedic surgery," *International Journal of Computer Assisted Radiology and Surgery* 10 (6), 971–979, 2015.

[21] A. Karamalis, *Ultrasound Confidence Maps and Applications in Medical Image Processing*. PhD thesis, 2013.

[22] C.P. Loizou, C. Theofanous, M. Pantziaris, and T. Kasparis, "Despeckle filtering software toolbox for ultrasound imaging of the common carotid artery," *Computer Methods and Programs in Biomedicine* 114 (1), 109–124, 2014.

[23] Y. Yu and S. Acton, "Speckle reducing anisotropic diffusion," *IEEE Trans. on Image Proc*. 11 (11), 1260–1270, 2002.

[24] A. Buades, B. Coll, and J.-M. Morel, "Non-Local Means Denoising," *Image Processing On Line* 2011, 2011.

[25] P. Coupe, P. Hellier, C. Kervrann, and C. Barillot, "Nonlocal means-based speckle filtering for ultrasound images," *IEEE Trans. on Image Proc*. 18 (10), 2221–2229, 2009.

[26] C.-A. Deledalle, L. Denis, and F. Tupin, "Iterative weighted maximum likelihood denoising with probabilistic patch-based weights," *IEEE Trans. on Image Proc*. 18 (12), 2661–2672, 2009.

[27] K. Radlak and B. Smolka, "Adaptive non-local means filtering for speckle noise reduction," in *Computer Vision and Graphics*, vol. 8671 of LNCS, 518–525, 2014.

[28] N. Sharma and L. Aggarwal, "Automated medical image segmentation techniques," *Journal of Medical Physics* 35 (1), 3–14, 2010.
[29] N.R. Pal and S.K. Pal, "A review on image segmentation techniques," *Pattern Recognition* 26 (9), 1277–1294, 1993.
[30] D.L. Pham, C. Xu, and J.L. Prince, "Current methods in medical image segmentation 1," *Annual Review of Biomedical Engineering* 2 (1), 315–337, 2000.
[31] Z. Lin, J.S. Jin, and H. Talbot, "Unseeded region growing for 3d image segmentation," in *Selected papers from Pan-Sydney Area Workshop on Visual Information Processing* (VIP2000) (P. Eades and J. Jin, eds.) 2 of CRPIT, (Sydney, Australia), 31–37, ACS, 2001.
[32] C. Ledig, W. Shi, W. Bai, and D. Rueckert, "Patch-based evaluation of image segmentation," in *Proceedings of the IEEE Conference on Computer Vision and Pattern Recognition*, 3065–3072, 2014.
[33] J.K. Udupa, V.R. Leblanc, Y. Zhuge, C. Imielinska, H. Schmidt, L.M. Currie, B.E. Hirsch, and J. Woodburn, "A framework for evaluating image segmentation algorithms," *Computerized Medical Imaging and Graphics* 30 (2), 75–87, 2006.
[34] P. Jaccard, "The distribution of the flora in the alpine zone," *New Phytologist* 11 (2), 37–50, 1912.
[35] L.R. Dice, "Measures of the amount of ecologic association between species," *Ecology* 26 (3), 297–302, 1945.
[36] T. Sørensen, *A Method of Establishing Groups of Equal Amplitude in Plant Sociology Based on Similarity of Species Content and Its Application to Analyses of the Vegetation on Danish Commons*. Biologiske Skrifter // Det Kongelige Danske Videnskabernes Selskab, I kommission hos E. Munksgaard, 1948.